Flow past cylinders and spheres

Low $Re = \frac{Ud}{\nu} < 1$

No slip ⇒ vorticity ⇒ diffusion (w/o convection) away from surface as per Stokes results with fore/aft symmetry

Oseen: linearized convection results in fore/aft asymmetry but only marginal improvement $C_D = \frac{24}{Re}\left(1 + \frac{3}{16}Re\right)$

$Re > 1$ Oseen breaks down and vorticity increasingly confined behind cylinder/sphere

$Re > 4$ two eddies form, closed separation behind cylinder; laminar wake

Moderate $Re > 40$

Wake unstable and when reaches 10^2 wake oscillates with $\underline{u}$ periodic in time and downstream distance, i.e., Kármán vortex street: staggered rows of vortices with opposite rotation. von Kármán studied as superposition irrotational vortices and showed staggered vs. non-staggered stable only if the ratio of the distance between the vortices is $\frac{\Delta y}{\Delta x} = 0.28$. Vortices move downstream at speed less than free stream, which means slowly follow cylinder.

$40 < Re < 80$ separation bubble and vortex sheet do not interact L_{SB} increases.

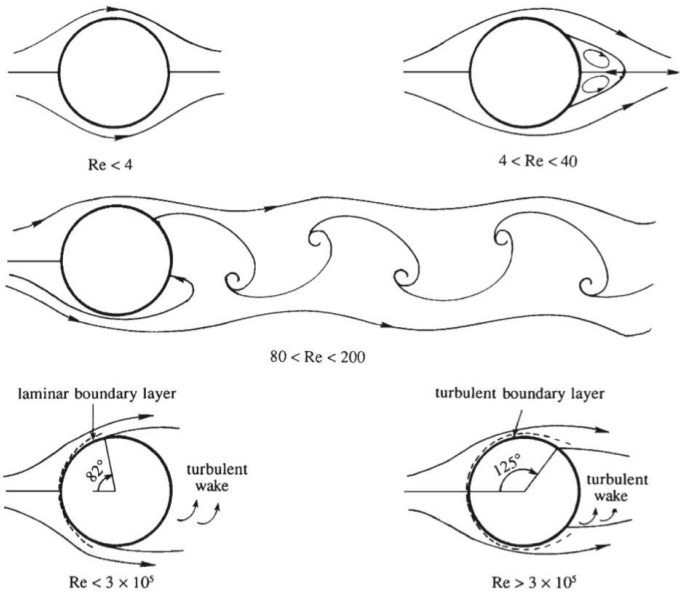

FIGURE 9.16 Depiction of some of the flow regimes for a circular cylinder in a steady uniform cross flow. Here $\mathrm{Re} = U_\infty d/\nu$ is the Reynolds number based on free-stream speed U_∞ and cylinder diameter d. At the lowest Re, the streamlines approach perfect fore-aft symmetry. As Re increases, asymmetry increases and steady wake vortices form. With further increase in Re, the wake becomes unsteady and forms the alternating-vortex von Karman vortex street. For Re up to $\mathrm{Re}_{cr} \sim 3 \times 10^5$, the laminar boundary layer separates approximately 82° from the forward separation point. Above this Re value, the boundary-layer transitions to turbulence, and separation is delayed to 125° from the forward separation point.

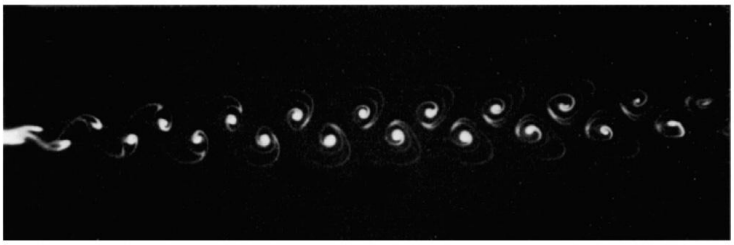

FIGURE 9.17 Von Karman vortex street downstream of a circular cylinder at $\mathrm{Re} = 55$. *Flow visualized by condensed milk. S. Taneda,* Jour. Phys. Soc., Japan **20**: *1714–1721, 1965, and reprinted with the permission of The Physical Society of Japan and Dr. Sadatoshi Taneda.*

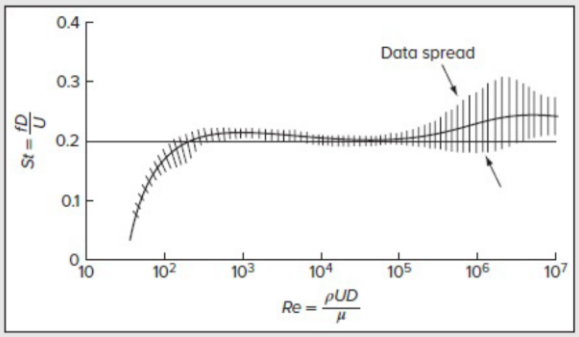

FIGURE 1-7

Measured Strouhal number for vortex shedding frequency behind a circular cylinder.

$Re > 80$ L_{SB} increases $\sim$2D and becomes unstable and oscillates as vortex street moves closer to cylinder. Attached eddies shed periodically from each side of cylinder alternately, resulting in alternating circulation and side force $\perp$ flow direction U_∞ at Strouhal number $St = \frac{\Omega d}{U_\infty}$. $C_{L,min} = 0$, $C_{L,\text{rms}} \neq 0$

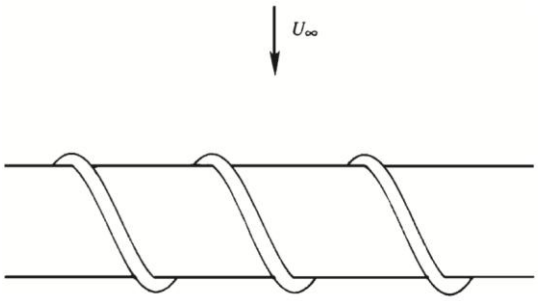

FIGURE 9.18 Spiral blades used for breaking up the span-wise coherence of vortex shedding from a cylindrical rod. Coherent vortex shedding can produce tonal noise and potentially large (and undesired) structural loads on engineered devices that encounter wind or water currents.

For small d and moderate U_∞ St in acoustic range: $U_\infty = 10$ m/s $d = 2$ mm $St = 0.2 \Rightarrow f = 1000$ cycles/s $\Rightarrow$ singing.

$Re < 200$ wake vortices laminar for long distances

$Re > 200$ vortex street unstable, irregular and chaotic flow between the vortices

At $Re > 3000$ St only evident near cylinder and wake fully turbulent for $x > 3D$

FIGURE 9.19 A von Karman vortex street downstream of mountain peaks in a strongly stratified atmosphere. There are several mountain peaks along the linear, light-colored feature running diagonally in the upper left-hand corner of the photograph. North is upward, and the wind is blowing toward the southeast. *R. E. Thomson and J. F. R. Gower,* Monthly Weather Review ***105****: 873–884, 1977; reprinted with the permission of the American Meteorological Society.*

High *Re*

$Re < 3 \times 10^5$ = 300,000: laminar BL, $\theta_s \approx 82^\circ$, base pressure ≈ constant < forebody pressure

C_D due $C_{Dp} \gg C_{Df}$ and since $\theta_s \approx$ constant. $C_D \approx$ constant up to $Re_{cr} \approx 3 \times 10^5$ = f(freestream TKE and roughness)

FIGURE 9.20 Surface pressure distribution around a circular cylinder at subcritical and supercritical Reynolds numbers. Note that the pressure is nearly constant within the wake and that the wake is narrower for flow at supercritical Re. The change in the top- and bottom-side, boundary-layer separation points near Re_{cr} is responsible for the change in C_p shown.

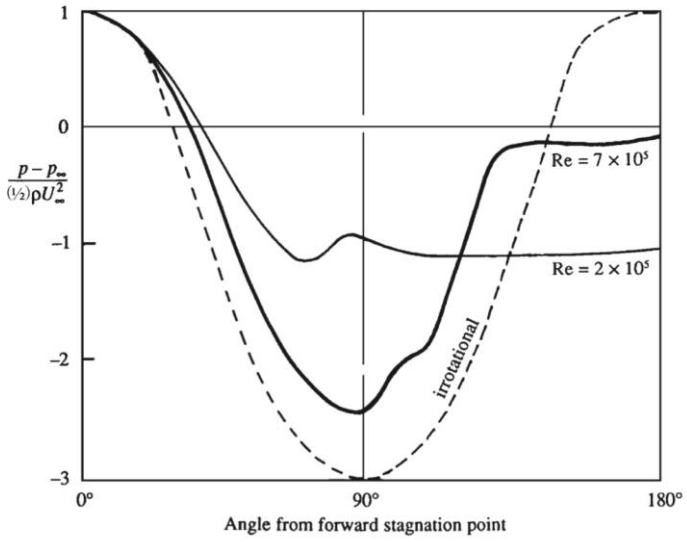

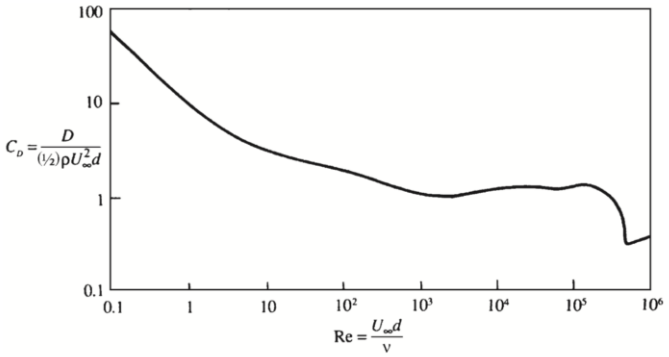

FIGURE 9.21 Measured drag coefficient, C_D, of a smooth circular cylinder vs. $\mathrm{Re} = U_\infty d/\nu$. The sharp dip in C_D near Re_{cr} is due to the transition of the boundary layer to turbulence, and the consequent downstream movement of the point of separation and change in the cylinder's surface pressure distribution.

$3 \times 10^5 < Re < 3 \times 10^6$ laminar BL transitions to turbulent BL, which is resistant separation such that $\theta_s \approx 125^\circ \Rightarrow$ thinner wake, reduced C_D, i.e., drag crisis with C_p closer potential flow. C_D drops from 1.2 to 0.33 at Re_{crit}

$Re > 3 \times 10^6$ θ_s reduces somewhat and C_D increases

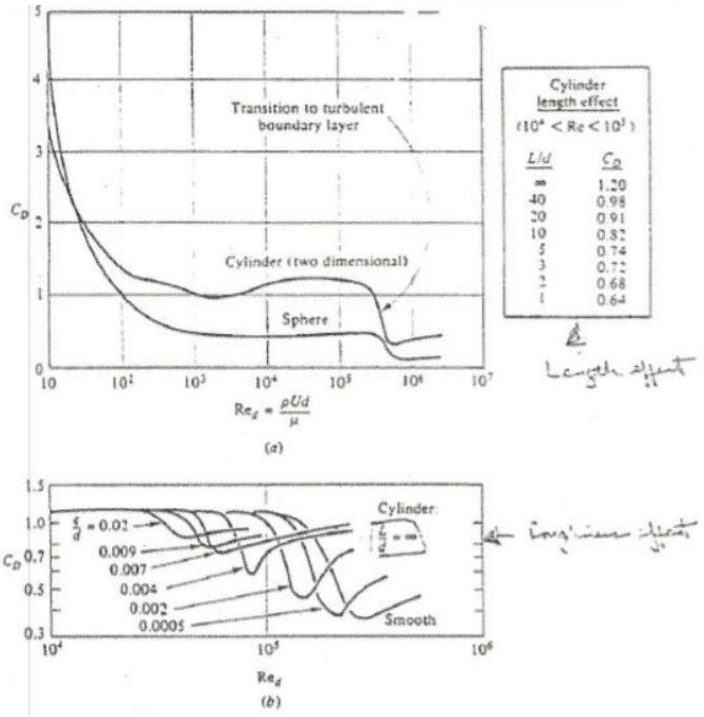

Fig. 5.3 The proof of practical dimensional analysis: drag coefficients of a cylinder and sphere: (a) drag coefficient of a smooth cylinder and sphere (data from many sources); (b) increased roughness causes earlier transition to a turbulent boundary layer.

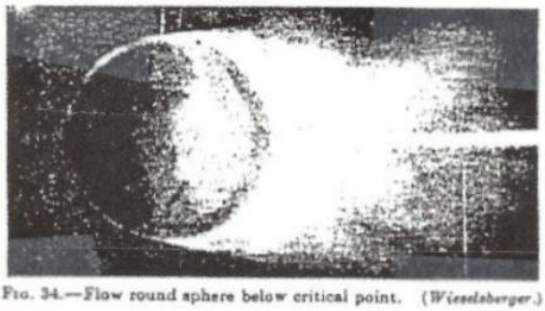

FIG. 34.—Flow round sphere below critical point. (*Wieselsberger.*)

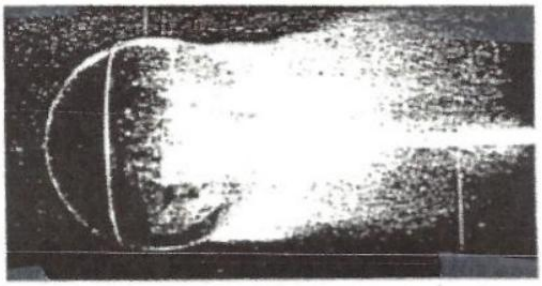

FIG. 35.—Owing to a thin wire ring round the sphere, the flow becomes of the other type with turbulent boundary layer. (*Wieselsberger.*)

Counter intuitive features:

1. $Re = \frac{Ud}{\nu}$

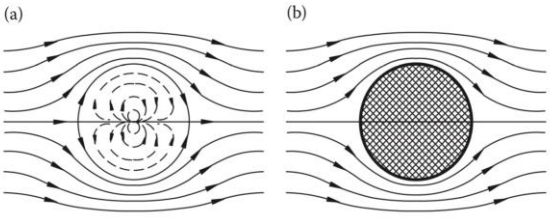

FIGURE 4.8
(a) Flow field represented by the complex potential $F(z) = U(z + a^2/z)$ and (b) flow around a circular cylinder of radius a.

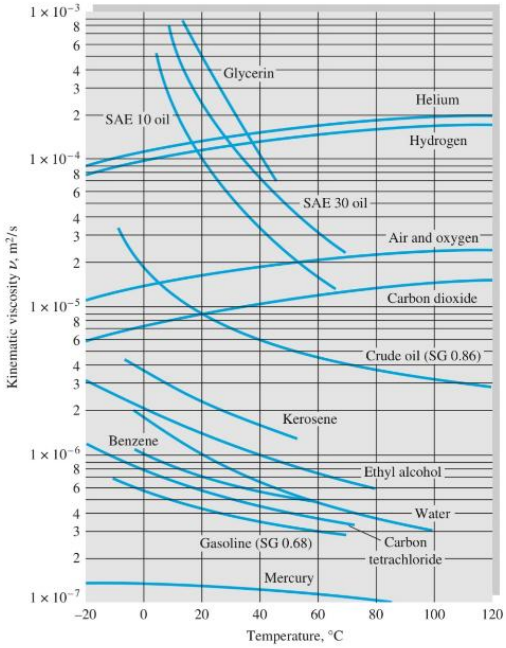

Fig. A.2 Kinematic viscosity of common fluids at 1 atm.

Ideal vs viscous flow, i.e., even very small viscosity $\neq 0$ has profound effects on flow due no-slip, BL, and separation, which induces asymmetry and C_D vs. slip, symmetry, and d'Alembert paradox $C_D = 0$

2. Symmetric geometry and BC can have asymmetric solutions

3. For range of *Re*, roughness, freestream TKE, etc., can reduce C_D due separation control, i.e., θs increases and narrower wake for smooth surface separation, e.g., cylinder and sphere.

VORTEX DYNAMICS IN THE CYLINDER WAKE

C. H. K. Williamson

Mechanical and Aerospace Engineering, Upson Hall, Cornell University, Ithaca, New York 14853

KEY WORDS: wakes, instability, vortex shedding

ABSTRACT

Since the review of periodic flow phenomena by Berger & Wille (1972) in this journal, over twenty years ago, there has been a surge of activity regarding bluff body wakes. Many of the questions regarding wake vortex dynamics from the earlier review have now been answered in the literature, and perhaps an essential key to our new understandings (and indeed to new questions) has been the recent focus, over the past eight years, on the three-dimensional aspects of nominally two-dimensional wake flows. New techniques in experiment, using laser-induced fluorescence and PIV (Particle-Image-Velocimetry), are vigorously being applied to wakes, but interestingly, several of the new discoveries have come from careful use of classical methods. There is no question that strides forward in understanding of the wake problem are being made possible by ongoing three-dimensional direct numerical simulations, as well as by the surprisingly successful use of analytical modeling in these flows, and by secondary stability analyses. These new developments, and the discoveries of several new phenomena in wakes, are presented in this review.

Annu. Rev. Fluid. Mech. 1996. 28:477–539

Applied Ocean Research 59 (2016) 663–675

Contents lists available at ScienceDirect

Applied Ocean Research

journal homepage: www.elsevier.com/locate/apor

Large-eddy simulation of the flow past a circular cylinder at sub- to super-critical Reynolds numbers

Seong Mo Yeon, Jianming Yang, Frederick Stern*

IIHR-Hydroscience and Engineering University of Iowa, Iowa City, IA 52242, USA

ARTICLE INFO

Article history:
Received 26 January 2015
Received in revised form 5 October 2015
Accepted 12 November 2015
Available online 23 December 2015

Keywords:
Large-eddy simulation
Circular cylinder
Critical Reynolds number
Drag crisis
Verification and validation

ABSTRACT

Large-eddy simulation of turbulent flow past a circular cylinder at sub- to super-critical Reynolds numbers is performed using a high-fidelity orthogonal curvilinear grid solver. Verification studies investigate the effects of grid resolution, aspect ratio and convection scheme. Monotonic convergence is achieved in grid convergence studies. Validation studies use all available experimental benchmark data. Although the grids are relatively large and fine enough for sufficiently resolved turbulence near the cylinder, the grid uncertainties are large indicating the need for even finer grids. Large aspect ratio is required for sub-critical Reynolds number cases, whereas small aspect ratio is sufficient for critical and super-critical Reynolds number cases. All the experimental trends were predicted with reasonable accuracy, in consideration the large facility bias, age of most of the data, and differences between experimental and computational setup in particular free stream turbulence and roughness. The largest errors were for under prediction of turbulence separation.

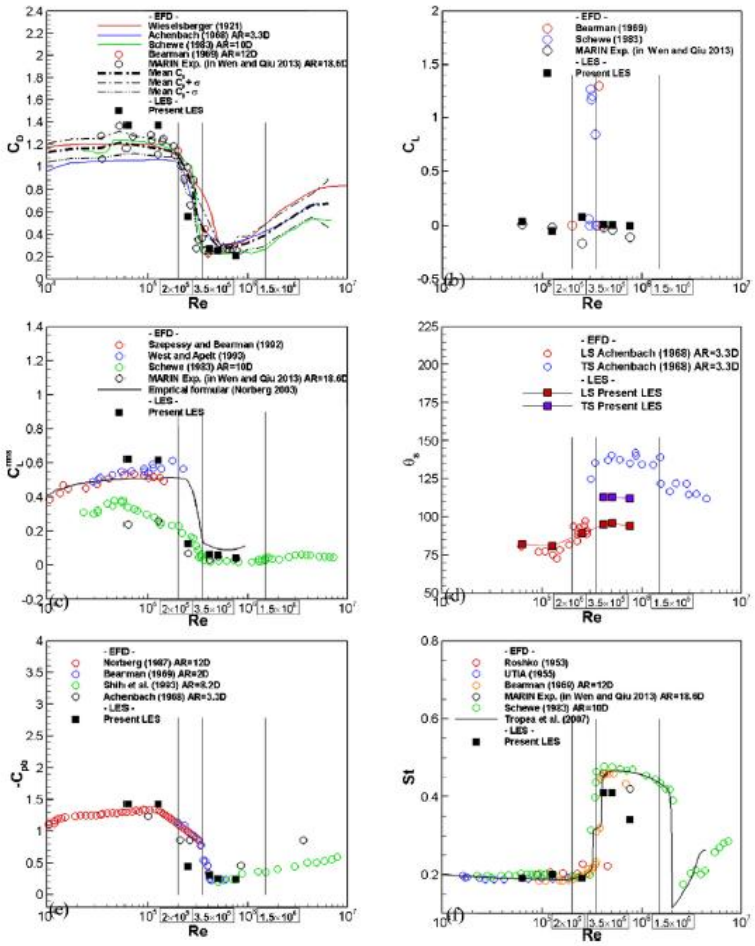

Fig. 2. Drag (a), lift (b), RMS lift (c) coefficients, separation angle (d), base pressure (e) and Strouhal number (f) as functions of Re.

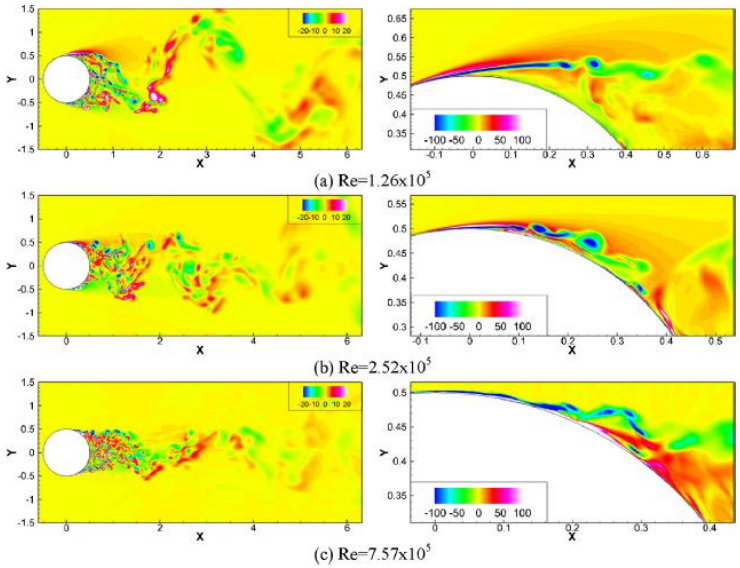

Fig. 7. Instantaneous spanwise vorticity contours, right side shows the close-up views.

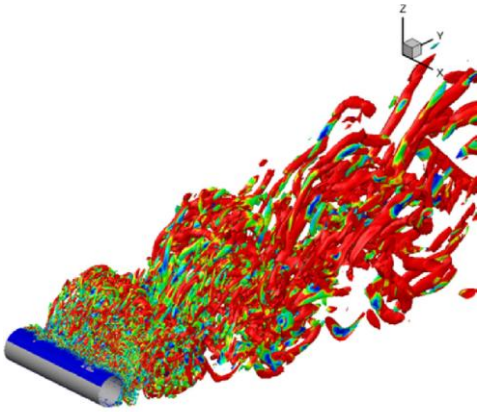

(a) sub-critical (Re=1.26x10^5)

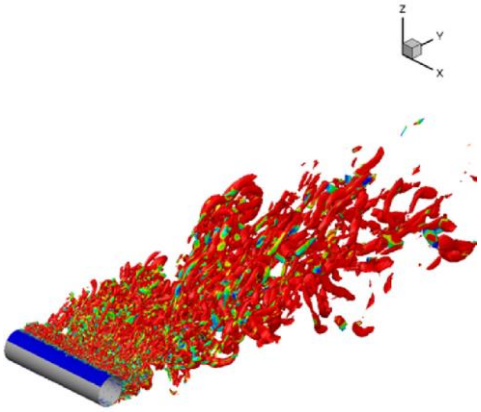

(b) critical (Re=2.52x10^5)

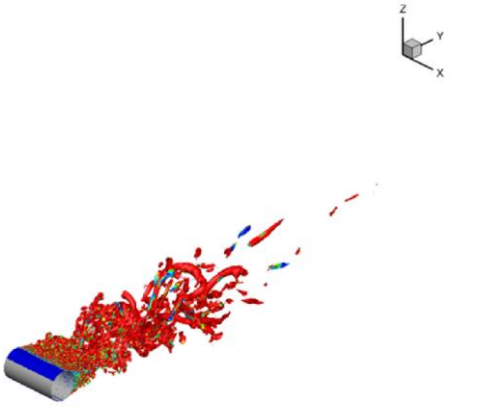

(c) super-critical (Re=7.57x10^5)

Fig. 8. Vortex structures with isosurfaces of Q-criterion colored by ν_t/ν.

Integrated High-Fidelity Validation Experiments and LES for a Surface-Piercing Truncated Cylinder for Sub and Critical Reynolds and Froude Numbers

Frederick Stern
IIHR-Hydroscience and Engineering University of Iowa
Iowa City, IA 52242
USA

frederick-stern@uiowa.edu

ABSTRACT

Integrated high-fidelity validation towing tank experiments and LES are presented for a surface-piercing truncated cylinder for sub- and critical Reynolds and Froude numbers, as a unit problem case study. The physics of interest are the effects of air-water interface on turbulence anisotropy and vortex shedding, 3D separation, transition to turbulence and the drag crisis; the effects of the truncated bottom; and ultimately bubble/droplet size distributions. The integrated experiments and LES was successful in using preliminary LES to guide the experiments especially for local flow surface pressure and flow field measurements. Experimental pacesetting issues were the difficulty of the PIV experiments; nonetheless, the data already collected is useful and valuable as the benchmark for LES validation. The largest hurdle in achieving the desired outcomes, however, was the LES since the current grid design and sizes required large computational resources. The experiments once completed will provide sufficient validation data for sub- and critical Re for many physics of interest. Experiments for spray droplet and air bubble size distribution measurements are still required. The LES at the current grid resolutions is able to fully-resolve the sub-critical but not the critical Re flow. Finer grids for critical Re are still required. Code development for overset grids, conservative convection schemes, and air/water interface LES models are also required. Future experiments and LES should focus on these issues along with extensions for VIV using towing tank PMM for pure sway motion.

NOMENCLATURE

AR	Aspect Ratio = L/D
C_D	Drag coefficient
C_L	Lift coefficient
C_{LRMS}	RMS lift coefficient
C_d	Sectional drag coefficient
C_l	Sectional lift coefficient
C_p	Pressure coefficient
D	Cylinder diameter
E	Comparison error = (D-S)%D where D and S are data and simulation values
f_k	Karman shedding frequency
f_{SL}	Shear layer frequency
Fr	Froude number =$U/(gD)^{1/2}$
k	Turbulent kinetic energy
U_C	Towing carriage speed

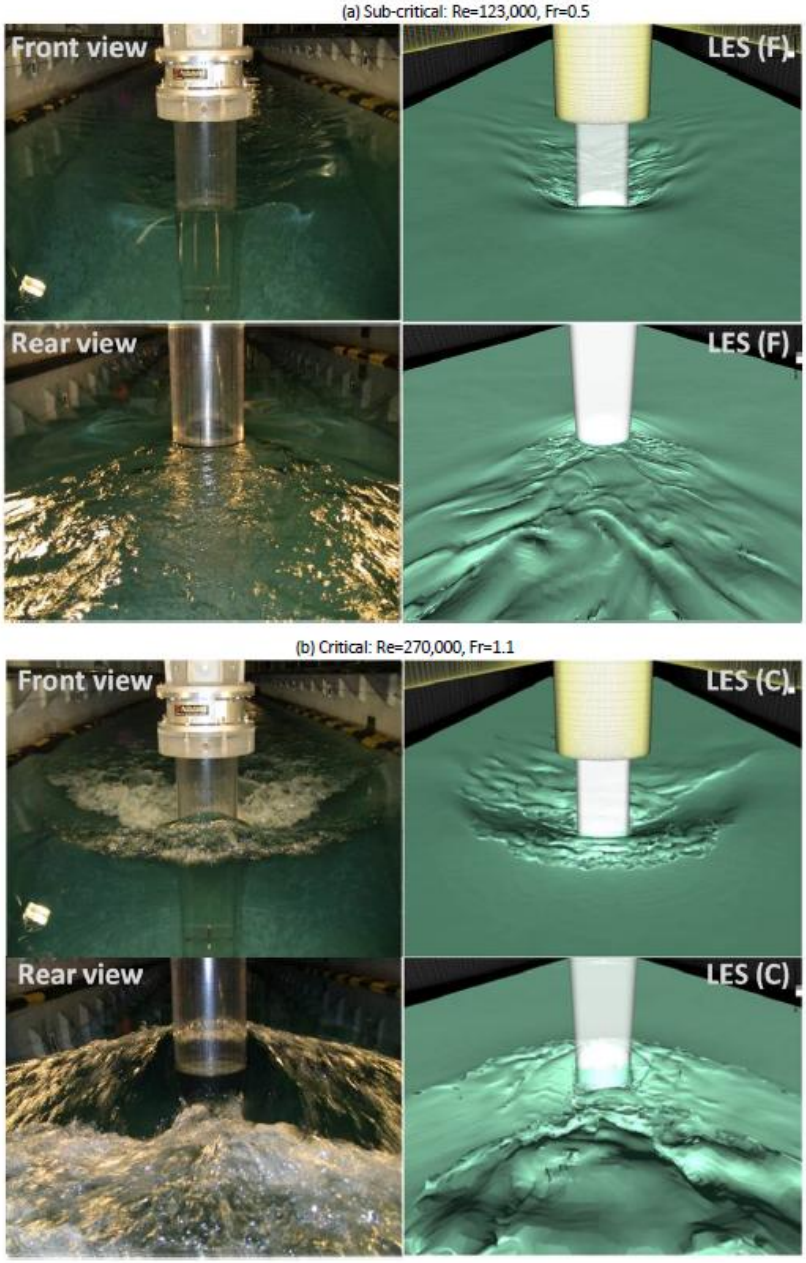

Figure 11-8: Photos of free surface waves around the cylinder model and comparisons with CFD simulations.

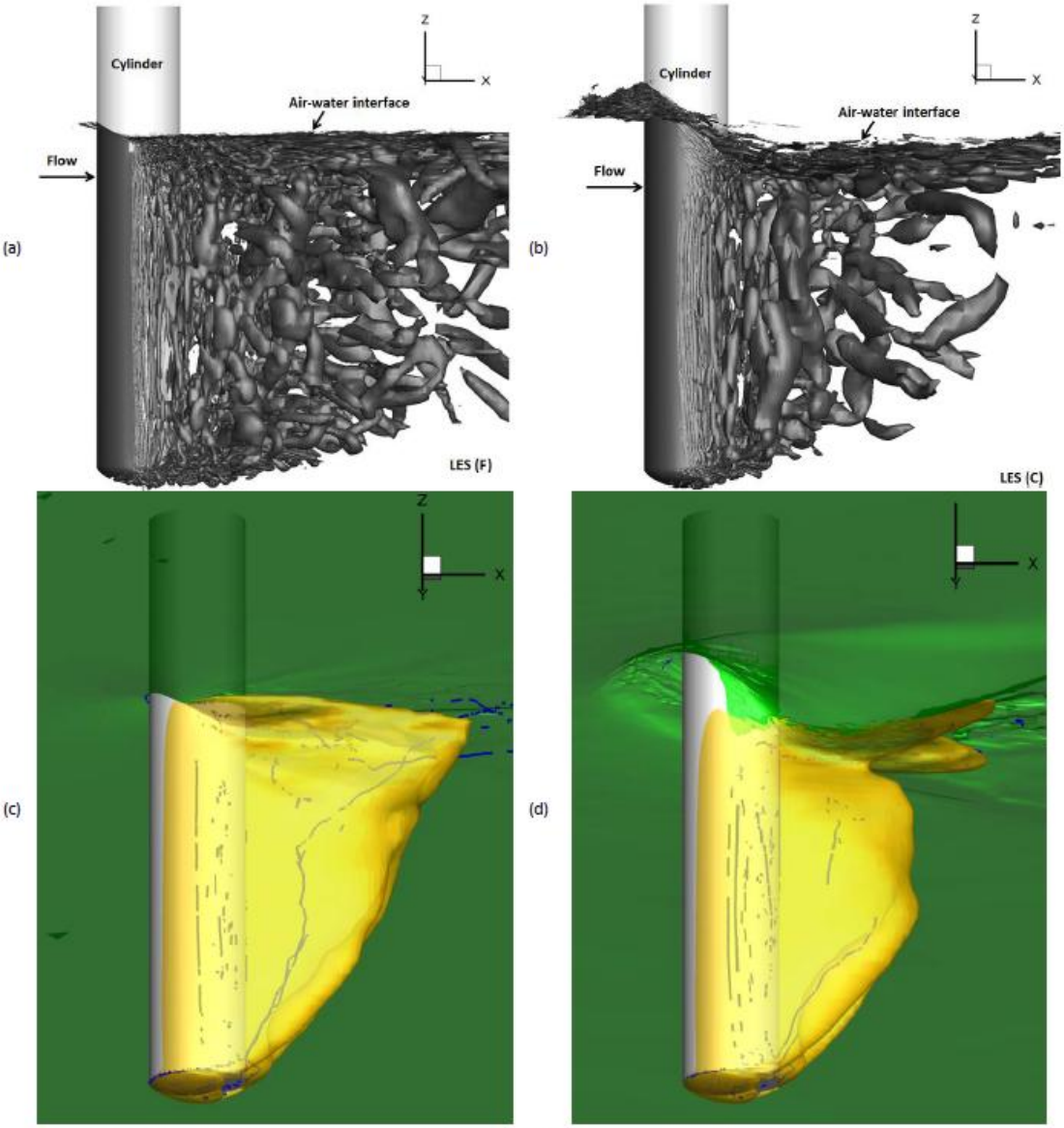

Figure 11-19: Iso-surface of instantaneous Q-criterion (Q=2): (a) sub-critical Re, (b) critical Re; Mean flow separation pattern with vortex core line: visualized approximately using the iso-surfaces of the stagnation C_P=-0.3, (c) sub-critical Re, (d) critical Re.

Effects of Sway Motion on Smooth-Surface Vortex Separation Onset and Progression: Surface Combatant and Surface-Piercing Truncated Cylinder

Frederick Stern
IIHR-Hydroscience and Engineering University of Iowa
Iowa City, IA 52242
USA

frederick-stern@uiowa.edu

ABSTRACT

The effects of sway motion on smooth-surface vortex separation onset and progression is studied for both practical surface combatant 5415 and basic surface-piercing truncated cylinder geometries. Towing tank experiments include PMM force and moment measurements and for the surface combatant TPIV for the bow region and preliminary 4D-PTV. LES simulations for subcritical Reynolds and Froude numbers are conducted for the cylinder. The sway amplitudes and frequencies are based on previous 5415 and single-phase cylinder studies. TPIV results show the major vortices dynamic onset and progression with alternating strengths and signs in time and trajectories in space. At phases 0° and 90°, the results exhibit similarity with static drift β=0 (straight ahead) and 10°, respectively. At the intermediate phases, the measurements show transition between these two conditions and substantial vortex interactions and unsteady separation for dynamic maneuvering. Vortex core analysis using Q criteria of the sonar dome vortices shows sinusoidal oscillation with 1st-order harmonic amplitude decreasing with progression. The core trajectory is loop-shaped but exhibits rather complicated shape changes along the vortex progression. The cylinder results show similarities with single phase studies, but with substantial free surface effects. Drag and lift show increase with amplitude and frequency with phase jump at frequency ratio fr=1 due to switch from 2P to 2S vortex shedding. Medium grid LES shows good agreement for force amplitudes, phases and FFT and phased averaged frequencies, which provides confidence in the flow field predictions, which are analyzed and compared with precursory straight-ahead experiments and LES; and single-phase controlled oscillation results. The 5415 results are being used by NATO AVT-253 for assessment of predictions methods and the cylinder results are being used for analysis of the physics of free surface boundary layer and wake/wave interactions and turbulence anisotropy; and for guidance for the analysis of the 5415 results. 4D-PTV for 5415 and finer LES grids for the cylinder are in progress.

1.0 INTRODUCTION

Smooth-surface vortex separation onset and progression is a ubiquitous flow feature and critical limiting factor for the design and operation of sea and air vehicles. Improvements in modeling and simulation capability are required to meet increased performance requirements and standardization of maritime regulations. For small amplitude static and dynamic maneuvers, both systems-based and physics-based CFD simulation method predictions are satisfactory; however, for large amplitude motions both approaches have difficulties, as shown by the results of the SIMMAN 2008 and 2014 Workshops (Stern et al., 2011; Simonsen et al., 2017).

Under the auspices of the AVT-183 Reliable Prediction of Separated Flow Onset and Progression for Air and Sea Vehicles significant progress was made for improved physical understanding and prediction capabilities for three-dimensional steady separation (NATO STO, 2017). The sea facet focused on large amplitude static drift β maneuvers for which benchmark validation experimental studies were conducted for surface combatant 5415 β=0, 10 and 20° (Yoon et al., 2014), KVLCC2 (very large crude carrier) β=30° (Abdel-Maksoud et al., 2015)

Figure 13 Schematics (left), PMM carriage (middle) and setup for surface piercing truncated cylinder (right)

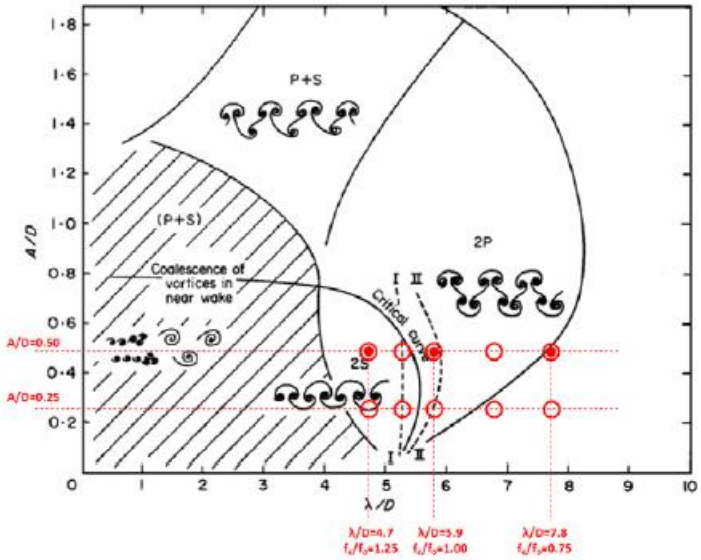

Figure 14 The map of regimes for vortex wake modes for controlled oscillating cylinder [Williamson and Roshko (1988), Williamson and Govardhan (2008)]; I, II are the curves where the forces on the body show a sharp "jump"; from Bishop and Hassan (1964). I is for wavelength decreasing and II is for wavelength increasing.

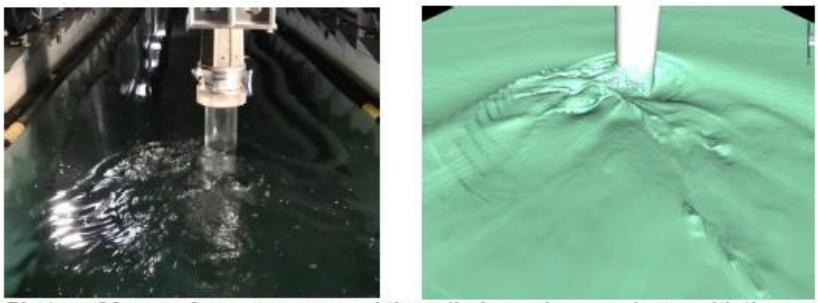

Figure 17 Photos of free surface waves around the cylinder and comparisons with the present LES simulations for (Re, Fr, AR, GR) = (123,000, 0.5, 4T, M) at $y=y_{max}$. (fr=1.25)

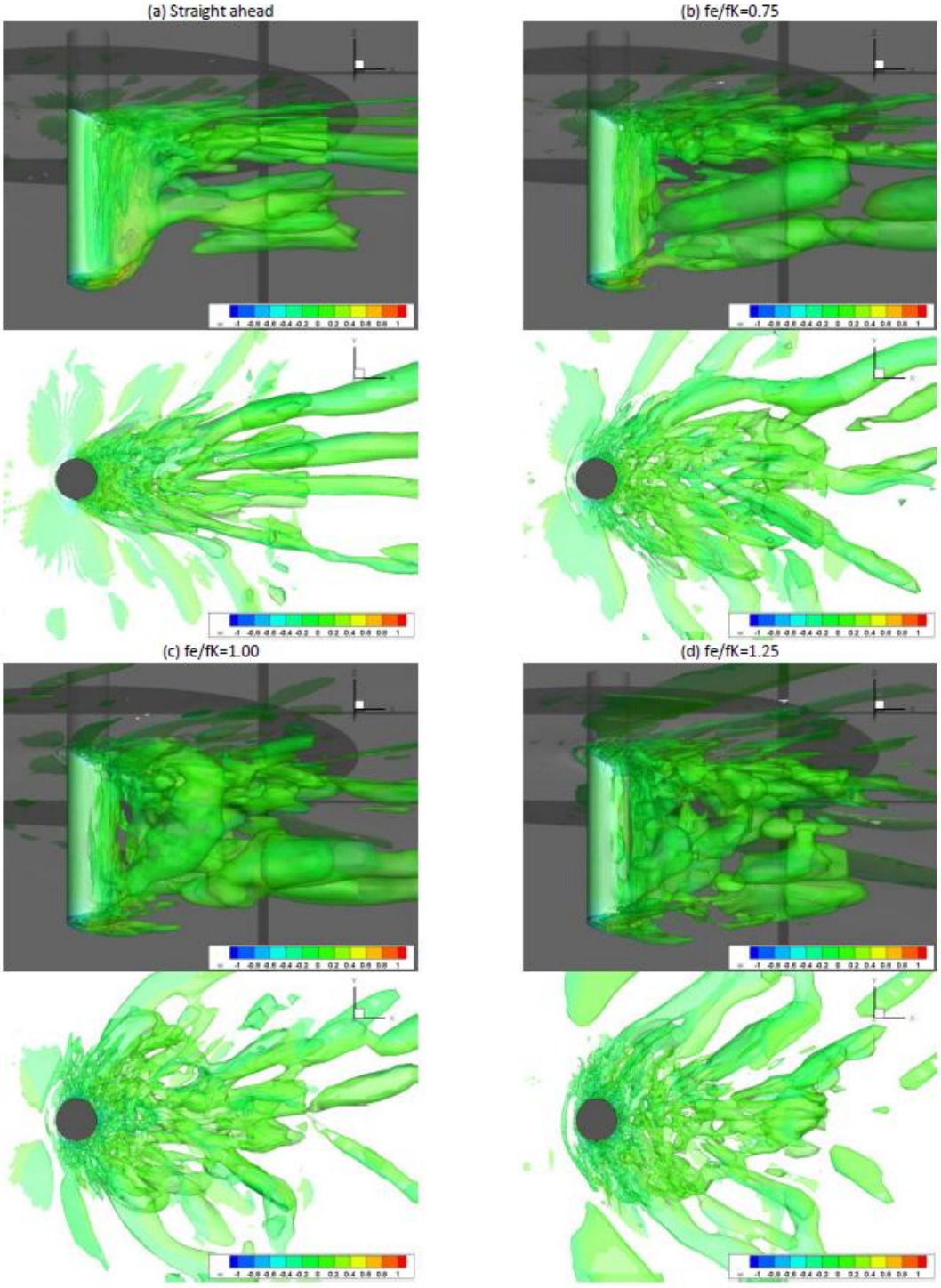

Figure 21 Iso-surface of mean Q-criterion (Q=0.04) for (Re, Fr, AR, GR)=(123,000, 0.5, 4T, M): (a) straight ahead, (b) fe/fK=0.75, (c) fe/fK=1.00, (d) fe/fK=1.25